Optimal filtering of polarisation-controlled Brillouin scattering in elliptical optophononic resonators

Elham Mehdi, A Rodriguez, P Priya, Edson Cardozo de Oliveira, Abdelmounaim Harouri, Isabelle Sagnes, L Le Gratiet, Martina Morassi, A Lemaître, Loïc Lanco, et al.

Optimal filtering of polarisation-controlled Brillouin scattering in elliptical optophononic resonators

E. Mehdi[1,*], A. Rodriguez[1], P. Priya[1], E. R. Cardozo de Oliveira[1], A. Harouri[1], I. Sagnes[1], L. Le Gratiet[1], M. Morassi[1], A. Lemaître[1], L. Lanco[2], M. Esmann[1], and N. D. Lanzillotti-Kimura[1]

[1]Université Paris-Saclay, CNRS, Centre de Nanosciences et de Nanotechnologies, 91120, Palaiseau, France
[2]Université Paris-Cité, CNRS, Centre de Nanosciences et de Nanotechnologies, 91120, Palaiseau, France

ABSTRACT

Accessing acoustic phonons at high frequencies in nanostructures becomes more and more essential in nanoelectronics, nano- and opto-mechanics and quantum technologies, as phonons can strongly interact with electrons and photons at the nanoscale. In spontaneous Brillouin scattering processes, the scattered photons energy, direction and polarisation are constrained by selection rules for a given input state. These selection rules are usually considered as intrinsic material properties in crystalline solids and the polarisation of the scattered photons depends on the polarisation of the excitation. In this work, we use elliptical optophononic micropillar resonators to control these optical polarisation selection rules. The degeneracy of the optical cavity modes of circular micropillars is lifted due to the elliptical cross-section of the micropillars, leading to two cavity modes orthogonally polarised and split in energy. The optical field polarisation state will depend on both orthogonal cavity modes and their associated polarisation states. Therefore, an incident laser beam linearly polarised along the diagonal axis of the elliptical pillar undergoes a wavelength dependent polarisation rotation. By choosing the polarisation and wavelength of the incident laser, we demonstrate that the polarisation state of the incident and reflected laser and the Brillouin scattering signal are different. In this way, background-free spontaneous Brillouin scattering spectra can be efficiently measured in a cross-polarisation scheme down to 18 GHz. Here, we theoretically and experimentally explore the optimal conditions for the polarisation and wavelength of the incident laser, and the ellipticity of the micropillars, to improve the polarisation-based filtering applied to Brillouin spectroscopy.

Keywords: Nanophononics, Brillouin scattering, Micropillars

1. INTRODUCTION

High-frequency acoustic phonons have received a lot of attention due to the emergence of cavity optomechanics and promising applications in sensing, simulation, and quantum technologies.[1–4] Brillouin spectroscopy measuring schemes are developed to study confined acoustic phonons at ultrahigh frequencies in nanostructures. Standard Brillouin spectroscopy schemes are generally optimized for a fixed phonon frequency[5,6] and optical wavelength and are not suitable for accessing variable high frequencies in the GHz range. Raman spectroscopy, on the other hand, is not well adapted as the spectral shift between the laser and the signal would be too small. New techniques are developed to overcome those challenges, exploiting for example the double optical resonance of optical cavities,[7–10] or the diffraction pattern mismatch between the Brillouin scattering and the reflected laser to spatially filter the signal.[11] The concept we explore here is to use birefringent microstructures, such as optical nano-antennas,[12,13] photonic crystal fibers[14,15] or elliptical micropillars,[16,17] to modify the polarisation selection rules of the Brillouin scattering process.

In this work, we use elliptical micropillars cavities to control the polarisation of spontaneous Brillouin scattering. The anisotropy of the micropillar cross-section leads to two cavity eigenmodes with non-degenerate energies and orthogonal linear polarisations.[18,19] The micropillar birefringence induces a wavelength-dependent polarisation rotation of any input polarised light.[20,21] Therefore, the Brillouin scattering emission undergoes a different

*Corresponding author: elham.mehdi@c2n.upsaclay.fr

polarisation rotation than the incident excitation laser. We reported in our previous work[22] the theoretical and experimental demonstration of the manipulation of the Brillouin scattering polarisation with an excitation laser polarised along the linear polarisation $|D\rangle$. We explore here, through numerical simulations, the optimal excitation conditions in polarisation and energy, to reach a situation where the Brillouin signal and the reflected excitation laser emerge from the micropillar with two orthogonal polarisation states. Such situation would enable an efficient filtering of the excitation laser by implementing a cross-polarisation detection scheme.

2. CAVITY-INDUCED POLARISATION ROTATION

We study acousto-optical microcavities formed by two distributed Bragg reflectors (DBR) grown by molecular-beam epitaxy on a GaAs substrate.[22,23] The top and bottom DBRs are formed by 25 and 29 periods of $Ga_{0.9}Al_{0.1}As$/ $Ga_{0.05}Al_{0.95}As$ bilayers, respectively. The two DBRs enclose a resonant spacer of optical length $\lambda/2$ at $\lambda \sim 900\,\text{nm}$. From this planar acousto-optical cavity, elliptical micropillars are fabricated by electron-beam lithography. Figure 1.a shows a SEM image of a single elliptical micropillar, with its major and minor axes, m and n. The two cavity eigenmodes corresponds to the linear horizontal and vertical polarisation states, $|H\rangle$ and $|V\rangle$, associated to two non-degenerate wavelength $\lambda_{\text{cav},H}$ and $\lambda_{\text{cav},V}$.

The response in polarisation of the cavity is characterised by the polarisation-dependent complex relfection coefficients r_H and r_V:[24]

$$r_{H/V} = 1 - 2\eta_{\text{top},H/V} \frac{1}{1 - \dfrac{2i(\omega_{\text{in}} - \omega_{\text{cav}}^{H/V})}{\kappa_{H/V}}}. \tag{1}$$

These coefficients depend on ω_{in} and $\omega_{\text{cav},H/V}$, the energy of the incident light on the cavity and the energy of the cavity modes. In this formalism, we consider $\hbar = 1$. They also depend on the output coupling efficiency through the top DBR $\eta_{\text{top},H/V}$, defined as $\eta_{\text{top},H/V} = \kappa_{\text{top},H/V}/\kappa_{H/V}$ with $\kappa_{\text{top},H/V}$ the top DBR damping rate and $\kappa_{H/V}$ the total cavity damping rate which includes leakage from the bottom and top DBRs, and the sidewall losses. This set of parameters ($\eta_{\text{top},H/V}$, $\kappa_{H/V}$ and λ_{cav}, H) can be experimentally retrieved from the measurement of the optical reflectivity of the cavity. An input laser polarised along one of the cavity modes is sent to the micropillar, and the reflected light is then measured as a function of the input laser wavelength λ_{laser}. The reflectivty spectra are finally fitted by taking the value of $|r_{H/V}|^2$ for each mode as shown in Figures 1.b, 1.c and 1.d for three micropillars of different elliptical cross-section. For each micropillar, the reflectivity is experimentally measured as a function of λ_{laser} and plotted as a function of $\lambda_{\text{cav}} - \lambda_{\text{laser}}$, with $\lambda_{\text{cav}} = (\lambda_{\text{cav},H} + \lambda_{\text{cav},V})/2$. Each simulated reflectivity is calculated with Eq. (1) and the corresponding cavity parameters, so that the simulation (line) fits the experimental points (circle). We define as well the cavity splitting $\Delta\lambda$ between the two modes, which characterises the birefringence of the cavity.

We consider an input polarisation state corresponding to the polarisation $|\psi_{\text{in}}\rangle$ of the excitation laser right before the micropillar. This state is associated to the Jones vector E_{in}:

$$E_{\text{in}} \propto \begin{pmatrix} b_{\text{in}}^H \\ b_{\text{in}}^V \end{pmatrix}, \tag{2}$$

with $b_{\text{in}}^{H/V}$ the polarisation-dependent average values of the input external field operators.[25] The laser reflected by the cavity undergoes a wavelength-dependent polarisation rotation. Its polarisation states becomes then $|\psi_{\text{out}}\rangle$, defined by the Jones vector E_{out}:

$$E_{\text{out}} \propto \begin{pmatrix} b_{\text{out}}^H \\ b_{\text{out}}^V \end{pmatrix}, \tag{3}$$

with $b_{\text{out}}^{H/V}$ the polarisation-dependent average values of the output external field operators.[25] The rotation polarisation of $|\psi_{\text{out}}\rangle$ is directly deduced from the reflexion coefficients $r_{H/V}$ given in (1) as

$$b_{\text{out}}^{H/V} = r_{H/V} \cdot b_{\text{in}}^{H/V}. \tag{4}$$

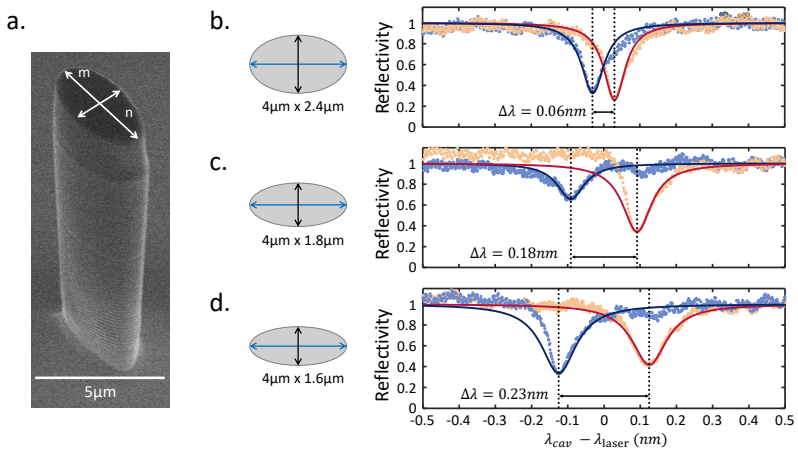

Figure 1. a. SEM image of an elliptical micropillar with m and n the major and minor axis of the cross-section respectively. b., c. and d. Experimental (circles) and simulated (lines) reflectivity spectra of three different micropillars cavity with various ellipticities. For each micropillar, the reflectivities of both cavity modes, H- and V-polarised, are plotted. Their respective cross-sections are drawn on the side.

3. BRILLOUIN SCATTERING POLARISATION ROTATION

The excitation laser generates Brillouin scattering in the cavity at energies ω_B^{S} and ω_B^{AS}, corresponding to the Stokes and the anti-Stokes signals respectively. We consider here only the first harmonic at $\pm 18\,\mathrm{GHz}$. The polarisation amplitude of the intracavity Brillouin scattering is the same as the input laser, howewer its polarisation state at the output of the cavity is rotated to the state $|\psi_{\mathrm{B}}\rangle_{\mathrm{B/AS}}$ due to the polarisation rotation induced by the cavity. This polarisation state corresponds to the Jones vector E_{B}:

$$E_{\mathrm{B}} \propto \begin{pmatrix} b_{\mathrm{B}}^{H} \\ b_{\mathrm{B}}^{V} \end{pmatrix}, \tag{5}$$

where b_{B}^{H} is the average value of the Brillouin scattering operator defined as follow:

$$b_{\mathrm{B}}^{H} \propto \frac{1}{1-\dfrac{2i(\omega_{\mathrm{B}}-\omega_{\mathrm{cav}}^{H/V})}{\kappa_{H/V}}} \cdot \frac{1}{1-\dfrac{2i(\omega_{\mathrm{in}}-\omega_{\mathrm{cav}}^{H/V})}{\kappa_{H/V}}} \cdot b_{\mathrm{in}}^{H/V}. \tag{6}$$

The Brillouin scattering polarisation depends therefore on the input polarisation state, defined by the amplitude $b_{\mathrm{in}}^{H/V}$, and on the cavity parameters as well. The first term in (6) describes the Brillouin scattering at the energy ω_{B}, while the second term describes the incoming laser beam at ω_{in}.

We now numerically calculate the Jones vector E_{out} and E_{B} as a function of the input laser wavelength λ_{laser} for different values of E_{in}. We note that the range of values of E_{in} are chosen to cover the whole Poincaré sphere. For every input polarisation described by its vector E_{in}, we then calulate the Stokes parameters associated to E_{out} and E_{B} as a function of λ_{laser}. From those Stokes parameters, giving the coordinates of the polarisation states in the Poincaré sphere, we deduce the angle θ between the polarisation states $|\psi_{\mathrm{out}}\rangle$ and $|\psi_{\mathrm{B}}\rangle_{\mathrm{B/AS}}$ in the Poincaré sphere. The angle θ depends on the wavelength of the input laser λ_{laser} and on the input polarisation state $|\psi_{\mathrm{in}}\rangle$. Finally, the ideal condition for the reflected laser to be entirely filtered out is to have the two polarisation states opposite to each other in the Poincaré sphere with an angle of $\theta = 180°$.

For a given input polarisation state $|\psi_{\mathrm{in}}\rangle$ and a given input laser wavelength λ_{laser}, we find the maximal angle θ_{max} reached between $|\psi_{\mathrm{out}}\rangle$ and $|\psi_{\mathrm{B}}\rangle_{\mathrm{B/AS}}$ for each micropillar. Such angle corresponds to an optimal filtering condition where the two polarisation states are maximally separated, thus the laser can partially be filtered out.

The quality of the filtering depends on how much the states are separated from each other. In figure 2, $|\psi_{\text{out}}\rangle$ and $|\psi_{\text{B}}\rangle_{\text{B/AS}}$ are plotted in the Poincaré sphere in the situation where the maximal angle θ_{max} is reached for the three different micropillars. The corresponding input polarisation state $|\psi_{\text{in}}\rangle$ is also plotted for each case. The top line of Poincaré spheres corresponds to the comparison between the output polarisation states of the reflected laser and the Stokes signal of the Brillouin scattering, while the bottom line compares the reflected laser to the anti-Stokes signal. We note that for one given micropillar, with its ellipticity, the optimal filtering condition (λ_{laser}, $|\psi_{\text{in}}\rangle$) are different for the Stokes and anti-Stokes signal.

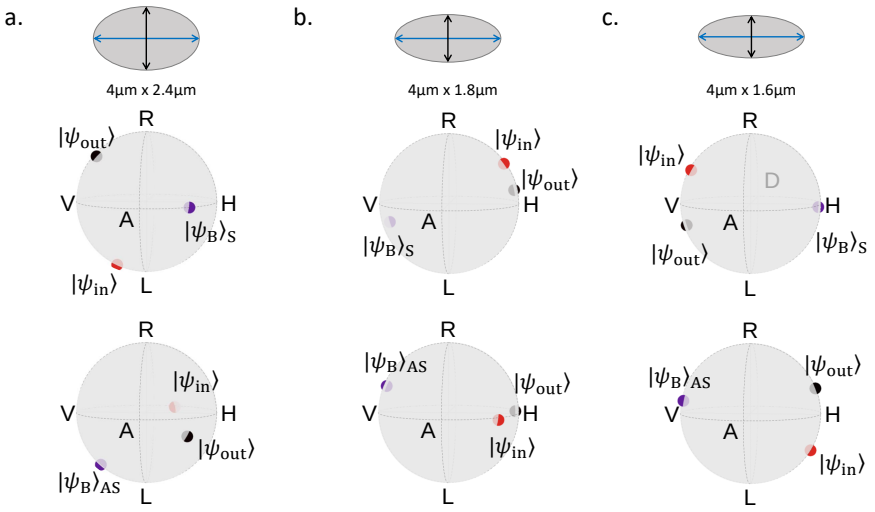

Figure 2. Comparison in the Poincaré sphere between the reflected laser polarisation state $|\psi_{\text{out}}\rangle$ and the Brillouin scattering polarisation state $|\psi_{\text{B}}\rangle_{\text{B/AS}}$ for three micropillars with different ellipticities (a., b., and c.). Each sphere corresponds to the optimal condition of $|\psi_{\text{in}}\rangle$ and λ_{laser} giving the maximal angle θ_{max} between $|\psi_{\text{out}}\rangle$ and $|\psi_{\text{B}}\rangle_{\text{B/AS}}$. In each situation, the corresponding $|\psi_{\text{in}}\rangle$ is also plotted in the Poincaré sphere.

For the first elliptical micropillar (Figure 2.a), the maximal angle reaches the values $\theta^{S}_{\text{max}} = 105°$ and $\theta^{AS}_{\text{max}} = 104°$ for the Stokes and anti-Stokes signals respectively. Under these conditions, the polarisation state of the reflected laser is not orthogonal to the Brillouin scattering polarisation states, and it cannot be entirely filtered out. The maximal angle reaches $\theta^{S}_{\text{max}} = 133°$ and $\theta^{AS}_{\text{max}} = 137°$ for the second micropillar (Figure 2.b), and goes up to $\theta^{S}_{\text{max}} = \theta^{AS}_{\text{max}} = 141°$ for the third micropillar (Figure 2.c). For the explored range, the maximal angle reached between the polarisation sates $|\psi_{\text{out}}\rangle$ and $|\psi_{\text{B}}\rangle_{\text{B/AS}}$ increases with the ellipticity of the pillar.

4. DISCUSSION

The ellipticity of a micropillar determines the splitting $\Delta\lambda$ between the two cavity modes,[26] which has an impact on the possible rotation of the polarisation states. Indeed, the cavity-induced polarisation rotation depends on the overlap in energy between the two optical cavity modes, which depends on the separation in energy of the two modes, given by $\Delta\lambda$, and on the full width at half maximum of the cavity as well, defined by the total cavity damping rate $\kappa_{H/V}$. A small overlap between the two cavity modes implies a bigger polarisation rotation, allowing $|\psi_{\text{out}}\rangle$ and $|\psi_{\text{B}}\rangle_{\text{B/AS}}$ to reach higher values of θ. While a large overlap results to smaller cavity-induced polarisation rotation and thus, smaller angles θ are reached.

For a given micropillar, optimal conditions can be reached as $|\psi_{\text{in}}\rangle$ and λ_{laser} can experimentally be tuned. However, the ellipticity of the micropillars has a great role in the polarisation rotation as a higher ellipticity allows to reach higher values of θ and thus achieve an efficient filtering of the laser. The shape of the micropillar cross-section can be designed with the fabrication process, as well as the total cavity damping rate $\kappa_{H/V}$, which also impacts the optimization of the filtering. The value of $\kappa_{H/V}$ depends on the number of layers in the DBRs,

and is limited by the fabrication process. The discussion in this work remains limited, as the numerical simulations takes only into account the polarisation rotation . Indeed, working with micropillar with high ellipticities can experimentally be limited as the spatial mode matching between the micropillar and the incoming beam would not be optimal, leading to a degraded coupling with the cavity. Under this condition, the Brillouin scattering is not efficient and of low intensity. Therefore, implementing this polarisation-based Brillouin spectroscopy technique requires to work with elliptical micropillars allowing a mode matching efficient enough to collect the photons from the Brillouin scattering and elliptical enough to separate their polarisation from the reflected laser.

We theoretically demonstrated in this work that the filtering of the Brillouin scattering can be achieved by exploiting the polarisation rotation induced by acousto-optical cavities in elliptical micropillars. Optimal conditions of filtering are reached for higher ellipticities. This technique is particularly relevant to study phonons in the $1\,\mathrm{GHz} - 1\,\mathrm{THz}$ range.

Acknowledgements

The authors gratefully acknowledge F. Pastier for taking the SEM images. The authors acknowledge funding from European Research Council Consolidator Grant No.101045089 (T-Recs). This work was supported by the European Commission in the form of the H2020 FET Proactive project No. 824140 (TOCHA), and the French RENATECH network.

REFERENCES

[1] Priya, Cardozo de Oliveira, E. R., and Lanzillotti-Kimura, N. D., "Perspectives on high-frequency nanomechanics, nanoacoustics, and nanophononics," *Appl. Phys. Lett.* **122**, 140501 (2023).

[2] Ortiz, O., Pastier, F., Rodriguez, A., Priya, Lemaitre, A., Gomez-Carbonell, C., Sagnes, I., Harouri, A., Senellart, P., Giesz, V., Esmann, M., and Lanzillotti-Kimura, N. D., "Fiber-integrated microcavities for efficient generation of coherent acoustic phonons," *Appl. Phys. Lett.* **117**, 183102 (2020).

[3] Ortiz, O., Priya, Rodriguez, A., Lemaître, A., Esmann, M., and Lanzillotti-Kimura, N. D., "Topological optical and phononic interface mode by simultaneous band inversion," *Optica* **8**(5), 598–605 (2021).

[4] Cardozo de Oliveira, E. R., Xiang, C., Esmann, M., Abdala, N. L., Fuertes, M. C., Bruchhausen, A., Pastoriza, H., Perrin, B., Soler-Illia, G. J. A. A., and Lanzillotti-Kimura, N. D., "Probing gigahertz coherent acoustic phonons in Tio2 mesoporous thin films," *Photoacoustics* **30**, 100472 (2023).

[5] Ike, Y., Tsukada, S., and Kojima, S., "High-resolution Brillouin spectroscopy with angular dispersion-type Fabry-Perot interferometer and its application to a quartz crystal," *Rev. Sci. Instrum.* **78**, 076104 (2007).

[6] Coker, Z., Troyanova-Wood, M., Traverso, A. J., Yakupov, T., Utegulov, Z. N., and Yakovlev, V. V., "Assessing performance of modern Brillouin spectrometers," *Opt. Express* **26**, 2400–2409 (2018).

[7] Trigo, M., Bruchhausen, A., Fainstein, A., Jusserand, B., and Thierry-Mieg, V., "Confinement of acoustical vibrations in a semiconductor planar phonon cavity," *Phys. Rev. Lett.* **89**, 227402 (2002).

[8] Lanzillotti-Kimura, N. D., Fainstein, A., Jusserand, B., and Lemaître, A., "Resonant Raman scattering of nanocavity-confined acoustic phonons," *Phys. Rev. B* **79**, 035404 (2009).

[9] Lamberti, F. R., Esmann, M., Lemaître, A., Gomez-Carbonell, C., Krebs, O., Favero, I., Jusserand, B., Senellart, P., Lanco, L., and Lanzillotti-Kimura, N. D., "Nanomechanical resonators based on adiabatic periodicity-breaking in a superlattice," *Appl. Phys. Lett.* **111**, 173107 (2017).

[10] Rodriguez, A., Priya, Ortiz, O., Senellart, P., Gomez-Carbonell, C., Lemaître, A., Esmann, M., and Lanzillotti-Kimura, N. D., "Fiber-based angular filtering for high-resolution Brillouin spectroscopy in the 20-300 GHz frequency range," *Opt. Express* **29**, 2637–2646 (2021).

[11] Esmann, M., Lamberti, F. R., Harouri, A., Lanco, L., Sagnes, I., Favero, I., Aubin, G., Gomez-Carbonell, C., Lemaître, A., Krebs, O., Senellart, P., and Lanzillotti-Kimura, N. D., "Brillouin scattering in hybrid optophononic Bragg micropillar resonators at 300 GHz," *Optica* **6**, 854–859 (2019).

[12] Curto, A. G., Volpe, G., Taminiau, T. H., Kreuzer, M. P., Quidant, R., and van Hulst, N. F., "Unidirectional emission of a quantum dot coupled to a nanoantenna," *Science* **5**, 930–933 (2010).

[13] O'Brien, K., Lanzillotti-Kimura, N. D., Rho, J., Suchowski, H., Yin, X., and Zhang, X., "Ultrafast acousto-plasmonic control and sensing in complex nanostructures," *Nat. Commun* **5**, 4042 (2014).

[14] Kang, M. S., Brenn, A., and Russell, P. S., "All-optical control of gigahertz acoustic resonances by forward stimulated interpolarization scattering in a photonic crystal fiber," *Physical Review Letters* **105**, 153901 (2010).

[15] Zeng, X., He, W., Frosz, M. H., Geilen, A., Roth, P., Wong, G. K. L., Russell, P. S., and Stiller, B., "Stimulated Brillouin scattering in chiral photonic crystal fiber," *Photon. Res.* **10**(3), 711–718 (2022).

[16] Sebald, K., Seyfried, M., Klembt, S., and Kruse, C., "Properties of photonic molecules and elliptical pillars made of ZnSe-based microcavities," *Opt. Express* **19**(20), 19422–19429 (2011).

[17] Wang, H., He, Y.-M., Chung, T.-H., Hu, H., Yu, Y., Chen, S., Ding, X., Chen, M.-C., Qin, J., Yang, X., Liu, R.-Z., Duan, Z.-C., Li, J.-P., Gerhardt, S., Winkler, K., Jurkat, J., Wang, L.-J., Gregersen, N., Huo, Y.-H., Dai, Q., Yu, S., Höfling, S., Lu, C.-Y., and Pan, J.-W., "Towards optimal single-photon sources from polarized microcavities," *Nat. Photonics* **13**, 770–775 (2019).

[18] Gayral, B., Gérard, J. M., Legrand, B., Costard, E., and Thierry-Mieg, V., "Optical study of GaAs/AlAs pillar microcavities with elliptical cross section," *Applied Physics Letters* **72**(12), 1421–1423 (1998).

[19] Whittaker, D. M., Guimaraes, P. S. S., Sanvitto, D., Vinck, H., Lam, S., Daraei, A., Timpson, J. A., Fox, A. M., Skolnick, M. S., Ho, Y.-L. D., Rarity, J. G., Hopkinson, M., and Tahraoui, A., "High Q modes in elliptical microcavity pillars," *Appl. Phys. Lett.* **90**, 161105 (2007).

[20] Antón, C., Hilaire, P., Kessler, C. A., Demory, J., Gómez, C., Lemaître, A., Sagnes, I., Lanzillotti-Kimura, N. D., Krebs, O., Somaschi, N., Senellart, P., and Lanco, L., "Tomography of the optical polarization rotation induced by a single quantum dot in a cavity," *Optica* **4**(11), 1326–1332 (2017).

[21] Hilaire, P., Antón, C., Kessler, C., Lemaître, A., Sagnes, I., Somaschi, N., Senellart, P., and Lanco, L., "Accurate measurement of a 96% input coupling into a cavity using polarization tomography," *Appl. Phys. Lett.* **12**, 201101 (2018).

[22] Rodriguez, A., Priya, Cardozo De Oliveira, E. R., Harouri, A., Sagnes, I., Pastier, F., Gratiet, L. L., Morassi, M., Lemaître, A., Lanco, L., Esmann, M., and Lanzillotti-Kimura, N. D., "Brillouin scattering selection rules in polarization-sensitive photonic resonators," *ACS Photonics* **10**, 1687–1693 (2023).

[23] Lamberti, F. R., Yao, Q., Lanco, L., Nguyen, D. T., Esmann, M., Fainstein, A., Sesin, P., Anguiano, S., Villafañe, V., Bruchhausen, A., Senellart, P., Favero, I., and Lanzillotti-Kimura, N. D., "Optomechanical properties of GaAs/AlAs micropillar resonators operating in the 18 GHz range," *Opt. Express* **25**(20), 24437–24447 (2017).

[24] Mehdi, E., Gundín, M., Millet, C., Somaschi, N., Lemaître, A., Sagnes, I., Le Gratiet, L., Fioretto, D. A., Belabas, N., Krebs, O., Senellart, P., and Lanco, L., "Giant optical polarisation rotations induced by a single quantum dot spin," *Nat. Commun.* **15**, 598 (2024).

[25] Gardiner, C. W. and Collett, M. J., "Input and output in damped quantum systems: Quantum stochastic differential equations and the master equation," *Phys. Rev. A* **31**, 3761 (1985).

[26] Gerhardt, S., Deppisch, M., Betzold, S., Harder, T. H., Liew, T. C. H., Predojevi, A., Höfling, S., and Schneider, C., "Polarization-dependent light-matter coupling and highly indistinguishable resonant fluorescence photons from quantum dot-micropillar cavities with elliptical cross section," *Phys. Rev. B* **100**, 115305 (2019).